Met. Mater. Int., Vol. 21, No. 2 (2015), pp. 350~355
doi: 10.1007/s12540-015-4245-9

Effects of Heat Input on the Pitting Resistance of Inconel 625 Welds by Overlay Welding

Jun Seok Kim[1], Young IL Park[2], and Hae Woo Lee[1,*]

[1]Department of Metallurgical Engineering, Dong-A University, Busan 604-714, Korea
[2]DNV GL Korea, Energy Korea Country Manager, Busan 612-824, Korea

(received date: 15 May 2014 / accepted date: 30 July 2014)

The objective of this study was to establish the relationship between the dilution ratio of the weld zone and pitting resistance depending on the heat input to welding of the Inconel alloy. Each specimen was produced by electroslag welding using Inconel 625 as the filler metal. In the weld zone of each specimen, dendrite grains were observed near the fusion line and equiaxed grains were observed on the surface. It was also observed that a melted zone with a high Fe content was formed around the fusion line, which became wider as the welding heat input increased. In order to evaluate the pitting resistance, potentiodynamic polarization tests and CPT tests were conducted. The results of these tests confirmed that there is no difference between the pitting resistances of each specimen, as the structures of the surfaces were identical despite the effect of the differences in the welding heat input for each specimen and the minor dilution effect on the surface.

Keywords: alloys, welding, corrosion, microstructure, scanning electron microscopy (SEM)

1. INTRODUCTION

The crude oil or gas recently obtained from the ocean floor contains chloride, H_2S and CO_2, which form a strongly corrosive environment, and the structures used to transport it must be made of an alloy with a strong corrosion resistance. Though these structures can be produced using a high-alloy steel with high corrosion resistance, such a process is inefficient in terms of processing and economic feasibility. As a means of resolving this, the overlay welding or cladding of an Inconel alloy sheet over the inside of carbon steel pipe may according to recent research be possible. Inconel alloy, a Ni-base alloy, is a super heat-resistant alloy of which the main alloy elements are Ni, Cr and Mo. As it has superior mechanical characteristics at high temperatures and strong corrosion resistance in diverse corrosive environments, it is used as a structural material for nuclear reactor steam generation engines and aircraft engines [1-12]. In addition, though Inconel alloy has good weldability and welding properties comparable to those of high-alloy steels, it is not widely used due to its high price [13-15].

Inconel alloy is used as a weld overlay for carbon steel pipe owing to the low yield strength of the Ni alloy. While the yield strength of carbon steel API 5l X65 is between 450 and 600 Mpa, the yield strength of Inconel 625, a Ni alloy, is 379 Mpa. Accordingly, carbon steel pipe can be turned into a structure which can meet stringent, required physical properties and corrosion resistance characteristics by weld-overlaying Inconel alloy. The low yield strength of Inconel alloy and the coefficients of the thermal expansion of the two metals are important factors. For AISI 304L, a large difference in the coefficients of thermal expansion of AISI 304L and carbon steel can cause thermal fatigue cracking and stress corrosion cracking. On the other hand, as Inconel 625 has a coefficient of thermal expansion similar to that of carbon steel, it is less susceptible to cracking than AISI 304L [16,17].

However, Inconel alloy has a disadvantage in that defects such as hot cracking, incomplete penetration and sensitization occur easily when it is welded, as there is no sufficient technical data related to welding materials, welding methods or welding conditions thus far. Also, when a temperature between 600 and 800 °C is used, Cr-Carbide ($M_{23}C_6$) is formed at the grain boundary, causing sensitization which becomes the starting point of corrosion. Accordingly, if the welding heat input is not properly controlled, the sensitization phenomenon occurs in the weld zone, causing the corrosion resistance of the Inconel ally to deteriorate.

The dilution ratio of the weld zone is also an important factor in overlay welding. When overlay welding is conducted using electroslag welding or submerged arc welding, of which the welding heat input is greater than those of other welding methods, the change in the composition of the weld zone caused by the dilution effect has an effect on the corrosion

*Corresponding author: hwlee@dau.ac.kr

resistance. Due to its high dilution ratio, the composition of the base material weld zone is diluted, causing the corrosion resistance to deteriorate because the phase and solidification mode of the weld zone change. At actual industrial sites, multi-layer welding is conducted, as single-layer welding is unable to meet the required corrosion resistance due to the high dilution effect, due to which the process becomes more complicated and the price increases. Accordingly, it is necessary to establish the relationship between the dilution ratio of the weld zone and the corrosion resistance more accurately [18-20].

In this paper, electroslag welding was conducted using Inconel 625 as the filler metal. The effects of the heat input on the microstructure were reviewed by producing specimens using three different welding heat inputs, and the effects of the dilution ratio and corrosion characteristics of Inconel alloy and the causes thereof were investigated.

2. EXPERIMENTAL PROCEDURES

2.1. Specimen preparation

In this study, a weld overlay process was conducted by electroslag welding using EQNiCrMo-3, the Inconel alloy specified in ASME, as the filler metal, and SA FB-2-CrMoNb, which is specified in EN 760 as the flux. The shape of the weld zone is shown in Fig. 1. The welding conditions of the specimens for an investigation of the characteristics which differ depending on the change in the welding condition are specified in Table 1. The welding heat input was setting by setting the voltage and speed at constant levels and controlling the amperage. Table 2 shows the composition of the carbon steel, the base material, and the composition of the Inconel strip. Table 3 shows the weld zone compositions of the specimens produced using the welding materials and in the welding conditions stated earlier. Each composition was measured using a spark emission spectrometer.

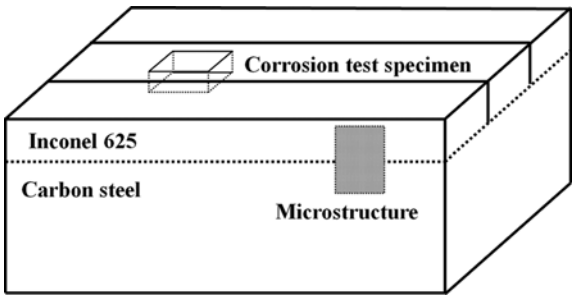

Fig. 1. Shape of the specimen.

2.2. Observation of the weld zone

In order to observe the microstructure of the weld zone, the surfaces of the weld zones were ground and polished using #600 ~ #1200, 1 μm and 0.04 μm of silica chloride, after which they underwent electrolysis etching for 60 seconds at 3 V using an etching liquid prepared at a volume ratio of $CH_3OH:HNO_3$ =17:2. The microstructures of the specimens were also observed and the compositions were measured using SEM and EDS.

2.3. Pitting resistance test

In order to determine the pitting resistance of each specimen, chemical tests and electro-chemical tests were conducted. As part of the electro-chemical test, potentiodynamic polarization tests were conducted. In order to observe the corrosion characteristics of Inconel alloy when it is used in a seawater environment, a polarization test was conducted in a Cl environment using an aqueous solution of 3.8%NaCl and 1 M HCl. In the corrosion cell used for the corrosion test, an Ag/AgCl, KCl (sat'd) electrode was used as the reference electrode and platinum foil was used as the counter electrode. Details of the test conditions are given in Table 4.

As the chemical test, the CPT tests (critical pitting temperature tests) specified in ASTM G8 were conducted. The

Table 1. Welding Condition of the Specimens

No.	Filler Metal Size	Polarity	Amperage	Voltage	Speed (cm/min)	Max.Heat Input (KJ/cm)
No.1			500			43.3
No.2	0.5T X 30W	DCRP	570	26	18	49.4
No.3			620			53.7

Table 2. Composition of the Filler and Base Metal (wt%)

	C	Mn	Si	Cr	Ni	Mo	Nb	Fe	Ti
Inconel Strip	0.015	0.1	0.1	22	Bal	9	3.6	0.3	0.23
Base metal	0.47	0.68	0.20	0.08	0.07	0.02	0.004	98.2	0.01

Table 3. Composition of the Specimens (wt%)

	C	Mn	Si	Cr	Ni	Mo	Nb	Fe	Ti
No.1	0.013	0.051	0.32	20.56	62.2	8.45	3.40	4.50	0.036
No.2	0.013	0.047	0.31	21.04	62.6	8.37	3.34	4.39	0.038
No.3	0.010	0.043	0.28	21.21	62.3	8.76	3.55	4.03	0.039

Table 4. Test Condition of the Potentiodynamic Polarization Test

Electrolyte	Temperature	Initial potential	Final potential	Scan rate
3.8% NaCl 1 M HCl	25 °C	-0.3 mV	1.3 mV	0.5 mV/sec

CPT test is a test that determines the pitting resistance of Ni-based alloys. It was conducted in accordance with ASTM G48 method C [21]. In order to observe corrosion on the surface after the test, the weld zone of each specimen was polished evenly. For the test, an aqueous solution of ferric chloride acidified by diluting 68.72 g of ferric chloride and 16 ml of 35% HCl with 600 ml of distilled water was used. The test method calls for the specimen to remain immersed in the aqueous solution of the ferric chloride for 72 hours while the temperature is maintained at the critical pitting temperature of the specimen. The critical pitting temperature of each specimen was determined by the equation below in accordance with the composition of the specimen.

$$CPT = 2.5\,Cr + 7.6\,Mo + 31.9\,N - 41.0 \quad (1)$$

The corroded surface of the specimen was cleaned 72 hours after it was immersed and the weight loss was measured before the surface was observed using a macro-microscope and SEM. The pitting resistance of each specimen was determined by analyzing the weight loss and corrosion form.

3. RESULTS AND DISCUSSION

3.1. Microstructure

Figure 2 shows the microstructure of the weld zone as observed using an optical microscope. Figure 2a shows an image of the fusion line and Figure 2b is an image of the microstructure near the surface. It was considered that, near the fusion line, a dendrite grain grew from the fusion line in the direction of the weld zone, as a dendritic pattern grew in the opposite direction as the flow of heat was pointed toward the base material when solidification took place. Moreover, an equiaxed grain was found to have been formed mainly near the surface. This is a solidification form which mainly appears in Inconel cladding steel materials. Lin [22] described that this type of solidification form has a dilution effect where, if the composition is changed by dilution, it has an effect on the solidification form as constitutional super-cooling takes place, causing growth and suppression of the crystal grain. Accordingly, it was presumed that the dendrite grain was generated as a result of the occurrence of constitutional super-cooling at the fusion line, where the dilution effect is relatively strong. However, though the dilution effect is weak near the surface of the weld zone, a minute equiaxed grain is presumed to have been generated due to the rapid cooling speed.

Figure 3 shows an image of the part near the fusion line as observed using SEM. In EDS images captured of the change in the composition from the nucleus of the dendrite to the matrix, large amounts of Nb, Ti and Mo were observed in the nucleus, most likely because solidification progressed gradually into a dendritic pattern after the metal compounds of Nb and Ti with a high melting point were preferentially

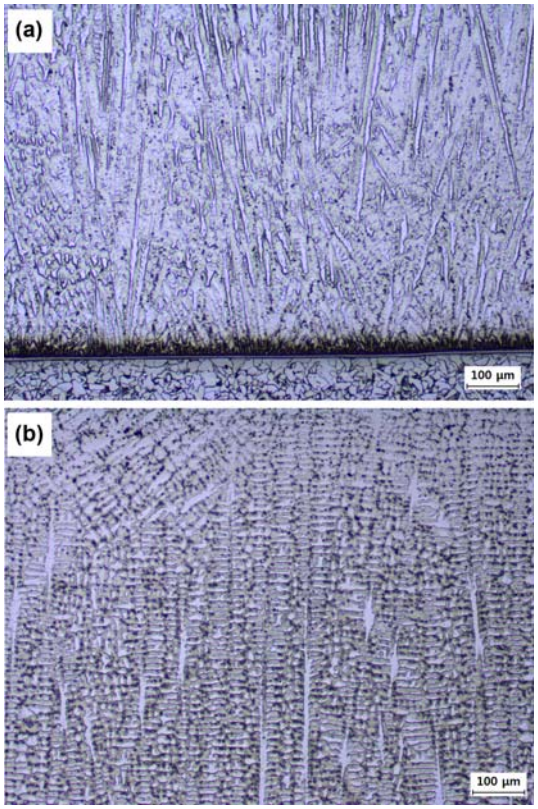

Fig. 2. Microstructure of weldment: (a) fusion line and (b) near the surface.

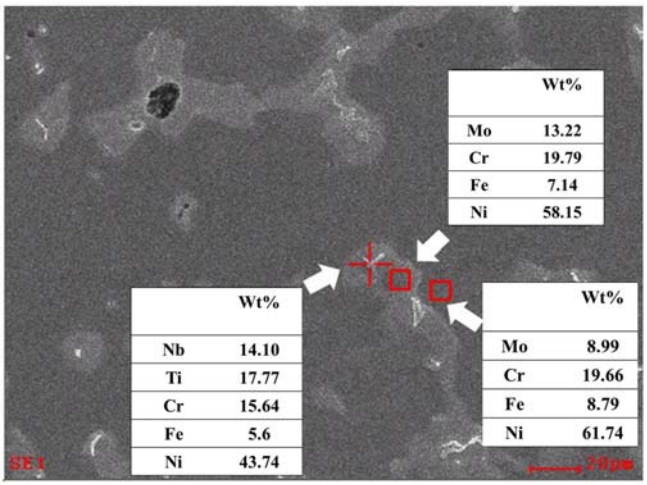

Fig. 3. SEM image of the part near the fusion line.

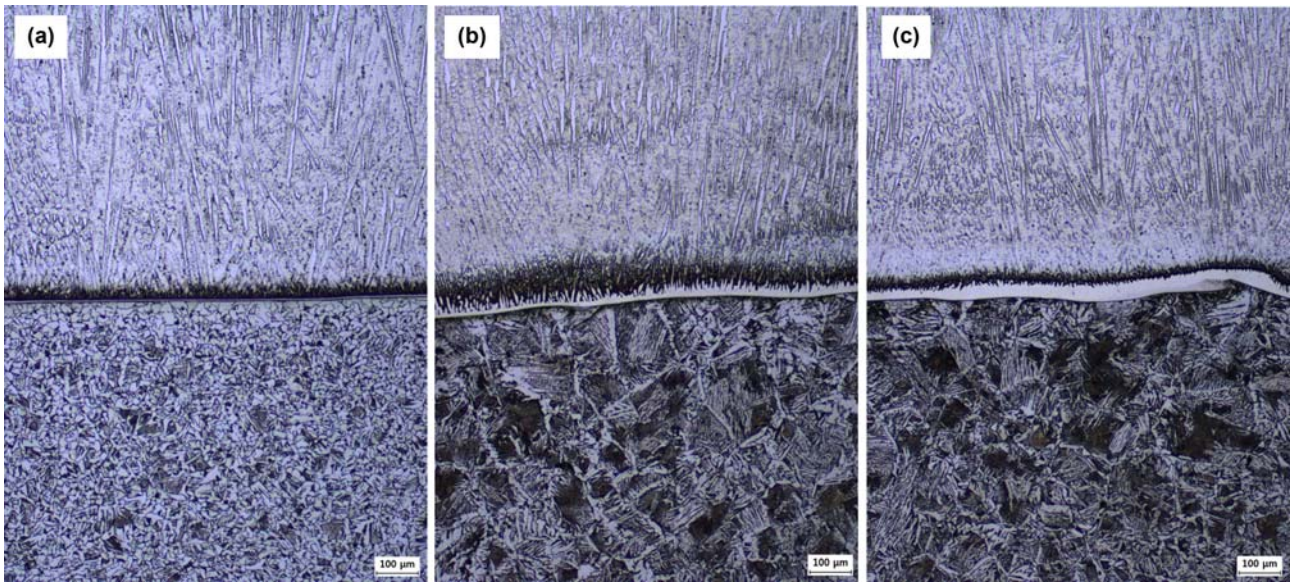

Fig. 4. Thin layer near the fusion line: (a) No. 1, (b) No. 2, and (c) No. 3

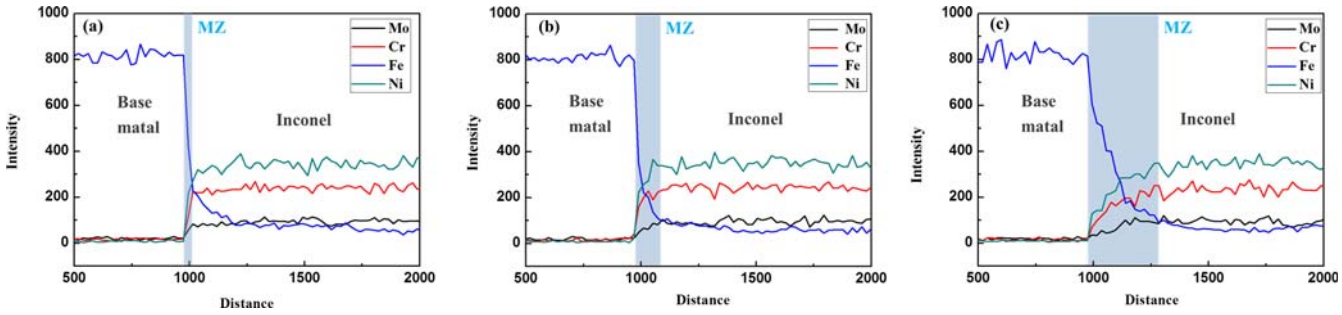

Fig. 5. The result of line mapping: (a) No. 1, (b) No. 2, and (c) No. 3.

precipitated. Also, the Fe content was found to be high in the matrix, most likely because the Fe in the base material was diluted into the weld zone, as the dilution effect of the fusion line was strong.

The differences in the specimens were observed near the fusion line. Figure 4 shows a thin layer observed near the fusion line, which is the melted zone formed by solidification after the Inconel strip was fully melted during the welding process. It was observed that as the heat input increases, the melted zone becomes wider. In particular, for specimen No. 3, for which the heat input is the highest, a partially melted zone could even be observed. Figure 5 shows the result of the measurement of the composition from the weld zone to the base material by means of line mapping, done in order to assess the change in the composition of the part near the fusion line. As shown in the graph in Fig. 5, a part is observed in which the Fe content is greater than the Ni content and the Cr content; this part is the melted zone of the fusion line. Accordingly, this part is thought to have been formed by the dilution of the base material Fe content into the weld zone as the welding heat input increased.

3.2. Pitting resistance test

Figure 6 shows the curves of the potentiodynamic polarization tests conducted in 3.8% NaCl solution and 1 M HCl. In both tests, the active passivation behaviors of all the specimens were found to be similar. Though there are minor differences in the current density and E_{pit} values, as they can be considered to be within the error range, it is confirmed that there is no difference between the pitting resistance levels of each specimen. In addition, Figure 7 is a photo showing the surface condition result of each specimen captured using a macro-microscope after the CPT test. The common corrosion trend of the specimens is that instances of pitting with depths shallower than 10 μm from the surfaces of the specimens are locally formed, with corrosion of the crevices occurring on the side of the specimen. However, no apparent pitting trend was found in any specimen. This result is rated as the first stage, the stage in which the pitting density is lowest and the pitting size is smallest, in accordance with the Standard Chart of ASTM G46 [23]. Also, Table 4 shows the weight loss ratio after the CPT test. Specimen No. 1 is shown to have the greatest reduction in weight, while speci-

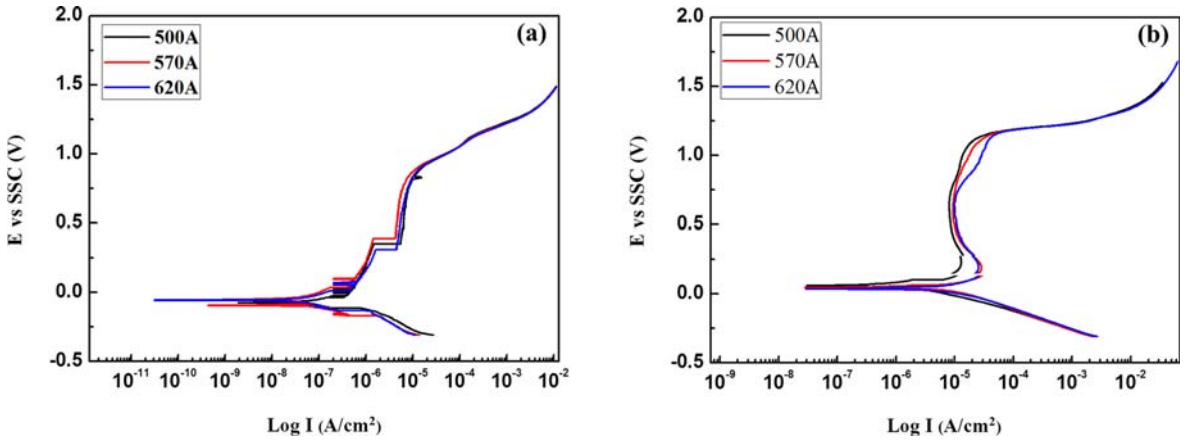

Fig. 6. Curves of the potentiodynamic polarization tests: (a) 3.8% NaCl and (b) 1 M HCl.

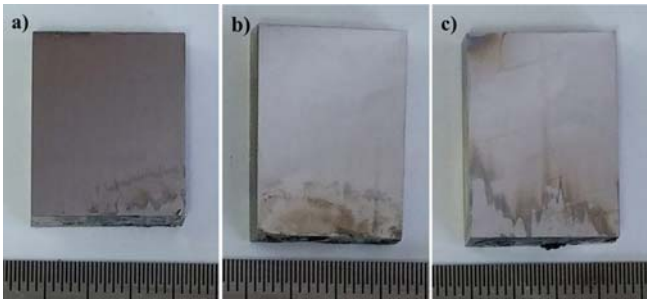

Fig. 7. The result of surface condition after the CPT test: (a) No. 1, (b) No. 2, and (c) No. 3.

men No. 3 shows the smallest reduction in weight. However, as the data is within the error range, it is presumed that it cannot easily be used to determine the pitting resistance.

The specimens of which the welding heat inputs were adjusted showed the same amount of corrosion resistance on account of the dilution rate of the surface. In the results of a study by Lin [22], the dilution rates of a bead bottom and a bead surface were found to be 55.35% and 4.5%, respectively, showing that the dilution rate of a surface is lower than that of its bottom. As the dilution effect of the surface is small, even when the welding heat input is adjusted, its effect on the surface is insignificant. The dilution rates of Cr and Mo measured on the surfaces of the specimens used in this test were below 7%, showing a result similar to those of earlier studies. Accordingly, the surface compositions of all specimens are nearly identical, and, as there is no difference in the Cr and Mo contents, each of which have an effect on the PREN, it is presumed that the differences in the pitting resistances between each of the specimens is insignificant. This also corresponds with the findings of earlier work conducted by Lee [24], in which an increase in the pitting potential was determined according to the Cr content.

4. CONCLUSION

(1) As a result of observing the microstructure of the weld zone, a dendrite grain was observed near the fusion line and an equiaxed grain was observed on the surface irrespective of the heat input. Also, a melted zone with a high Fe content was found to have formed near the fusion line. It was observed to become wider as the welding heat input increased.

(2) In the results of potentiodynamic polarization tests and CPT tests conducted in 3.8% NaCl solution and 1 M HCl, respectively, no difference was found between the pitting resistances of each specimens.

(3) Even if the welding heat inputs are different, as there is no difference in the composition because the dilution rate of a bead surface is remarkably slower than that of a bottom, it does not have a large effect on the PREN.

ACKNOWLEDGEMENT

This work was supported by the National Research Foundation of Korea (NRF) grant funded by the Korea government (MEST) (No. NRF-2014R1A2A2A01002776).

REFERENCES

1. W. F. Smith, *Structure and Properties of Engineering Alloy, 2nd ed.,* pp. 493-538, Kyobo Books, Korea (2009).
2. W. L. Mankins and S. Lamb, *Nickel and Nickel Alloys, 10th ed.*, p. 428, ASM International, USA (1990).
3. G. P. Airey, *Metallograghy*, **13**, 21 (1981).
4. R. A. Page and A. McMinn, *Metall. Trans. A* **17**, 877 (1986).
5. J. J. Kai, G. P. Yu, C. H. Tsai, M. N. Liu, and S. C. Yao, *Metall. Trans. A* **20**, 2057 (1989).
6. K. S. Kim, H. J. Lee, B. S. Lee, I. C. Jung, and K. S. Park, *Nucl. Eng. Des.* **239**, 2771 (2009).
7. H. Xue, Z. Li, Z. Lu, and T. Shoji, *Nucl. Eng. Des.* **241**, 731 (2011).

8. H.-J. Park and H.-W. Lee, *Korean J. Met. Mater.* **52**, 211 (2014).
9. W. Wu and C. H. Tsai, *Metall. Mater. Trans. A* **30A**(2), 417 (1999).
10. Y. T. Shin, H. S. Shin, and H. W. Lee, *Met. Mater. Int*. **18**, 1037 (2012).
11. J. M. Kim and H. W. Lee, *Met. Mater. Int*. **20**, 329 (2014).
12. J. M. Kim and H. W. Lee, *Korean J. Met. Mater*. **51**, 829 (2013).
13. Li Jian, C. Y. Yuh, and M. Farooque, *Corros. Sci.* **42**, 1573 (2000).
14. M. D. Mathew, P. Parameswaran, and K. Bhanu Sankara Rao, *Mater. Charact*. **59**, 508 (2008).
15. D. E. Jordan, *Weld world* **4**, 1 (1998).
16. S. K. Rai, and A. Kumar, *Scripta Mater.* **51**, 59 (2004).
17. Y. H. Lee and I. S. Kim, *Wear* **253**, 438 (2002).
18. Y. S. Ahn, B. H. Yoon, H. J. Kim, and C. H. Lee, *Met. Mater. Int.* **8**(5), 469 (2002).
19. T. E. Abioye, J. Folkes, and A. T. Clare, *J. Mater. Process. Technol.* **213**, 2145 (2013).
20. H. R. Zareie Rajani, S. A. A. Akbari Mousavi, and F. Madani Sani, *Mater. Des.* **43**, 467 (2013).
21. ASTM Standard G48, *Standard Test Methods for Pitting and Crevice Corrosion Resistance of Stainless Steels and Related Alloys by Use of Ferric Chloride Solution,* ASTM G-11 (Reapproved 2011).
22. C. M. Lin, *Surf. Coat. Technol.* **228**, 234 (2013).
23. ASTM Standard G46, *Standard Guide for Examination and Evaluation of Pitting Corrosion,* ASTM G46-94 (2005).
24. J. B. Lee, *Mater. Chem. Phys.* **99**, 224 (2006).